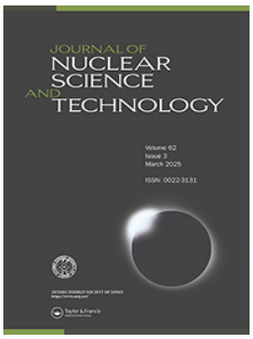

Journal of Nuclear Science and Technology

ISSN: 0022-3131 (Print) 1881-1248 (Online) Journal homepage: www.tandfonline.com/journals/tnst20

Evaluating the diffusion of Kr in UO_2 and ADOPT^{TM} using time-of-flight elastic recoil detection analysis (ToF-erda)

Robert J. W. Frost, Denise A. Lopes, Kyle D. Johnson, Sobhan Patnaik, Johan Oscarsson, Mauricio Sortica, Per Petersson & Daniel Primetzhofer

To cite this article: Robert J. W. Frost, Denise A. Lopes, Kyle D. Johnson, Sobhan Patnaik, Johan Oscarsson, Mauricio Sortica, Per Petersson & Daniel Primetzhofer (2025) Evaluating the diffusion of Kr in UO_2 and ADOPT^{TM} using time-of-flight elastic recoil detection analysis (ToF-erda), Journal of Nuclear Science and Technology, 62:3, 243-249, DOI: 10.1080/00223131.2024.2423639

To link to this article: https://doi.org/10.1080/00223131.2024.2423639

Published online: 18 Nov 2024.

JOURNAL OF NUCLEAR SCIENCE AND TECHNOLOGY
2025, VOL. 62, NO. 3, 243–249
https://doi.org/10.1080/00223131.2024.2423639

RAPID COMMUNICATION

OPEN ACCESS Check for updates

Evaluating the diffusion of Kr in UO_2 and ADOPT^{TM} using time-of-flight elastic recoil detection analysis (ToF-erda)

Robert J. W. Frost[a], Denise A. Lopes[b], Kyle D. Johnson[c], Sobhan Patnaik[b], Johan Oscarsson[d], Mauricio Sortica[d], Per Petersson[a,e] and Daniel Primetzhofer[a,d]

[a]Department of Physics and Astronomy, Uppsala University, Uppsala, Sweden; [b]Department of Physics, KTH Royal Institute of Technology, Stockholm, Sweden; [c]Studsvik Nuclear AB, Nyköping, Sweden; [d]The Tandem Laboratory, Uppsala University, Uppsala, Sweden; [e]Department of Electrical Engineering, KTH Royal Institute of Technology, Stockholm, Sweden

ABSTRACT

A combination of 300 keV ^{84}Kr ion implantation and Time-of-Flight Elastic Recoil Detection Analysis is utilised to investigate the diffusion of Kr in UO_2 and ADOPT^{TM} fuels. Composition depth-profiles on the nanometer scale were obtained, both for as-implanted samples and after annealing at 800°C for 1 h. Observed drifts in the ^{84}Kr profiles could be associated with short-range diffusion mechanisms. The approach employed here provides the possibility to make direct comparisons with atomistic scale modelling data, and can be of service as a separate effect test in line with the Accelerated Fuel Qualification initiative.

ARTICLE HISTORY
Received 16 May 2024
Accepted 23 October 2024

KEYWORDS
Kr implantation; ToF-ERDA; elemental depth-profiling; UO_2; ADOPT^{TM}

The diffusion of gaseous fission products such as Xe and Kr in nuclear fuel represents a significant performance and safety parameter due to their high fission-yields, high neutron absorption cross-sections and the potential to create pressure build up within fuel cladding, reducing the efficiency of heat rejection from the fuel, as well as potentially contributing to fuel fragmentation in high burnup fuel [1–3]. The study of the diffusion behaviour of these noble gas species, however, is an experimental challenge due, firstly, to difficulties in adding the gas species to the fuel matrix without causing additional modifications such as defects and, secondly, in accessing techniques which can monitor gas concentrations and diffusion on ultrashort-length scales. To date, the majority of diffusion parameters employed for UO_2 fuel performance analyses have been derived from irradiated material [4,5] either through measurements in the plenum, or by the annealing of fuel samples in a Materials Tests Reactor (MTR) or Post Irradiation Examination (PIE) facility, both of which require significant infrastructure and resources to operate and maintain, which have historically limited the number of samples available to establish correlations.

Nevertheless, these methods have contributed significantly to improving fuel performance, although bulk and grain-boundary thermal and athermal diffusion, as well as radial and axial temperature-variation in the fuel, are highly approximated and variable due to inherent differences in irradiation histories. Consequently, these methods do not produce the optimal benchmarking data for validation of low-scale atomistic models, such as Density Functional Theory (DFT) and Molecular Dynamics (MD), which contribute significantly to the Accelerated Fuel Qualification (AFQ) initiative [6]. AFQ relies strongly on physic-based models, such as the Simple Integrated Fission Gas Release and Swelling (SIFGRS) model integrated for UO_2 [7,8]. This model relies on low-length variables to physically describe the behaviour of gas species in the matrix (intragranular diffusion) and grain boundaries (intergranular diffusion) and has thermally-dependent variables such as D_0 (diffusion coefficient), activation energy, etc. [8]. Therefore, separate effect-tests that can validate the values obtained for such parameters are highly preferred over integral irradiation experiments due in no small part to dramatically reduced costs and delivery timescales [9].

Dedicated experimental work to decompose diffusion coefficients, has been undertaken by the nuclear fuel community [10,11]. The use of ion implantation at medium energies, followed by annealing and the detection of the implanted gas, has been performed using techniques such as Thermal-Desorption Spectrometry (TDS) [10] and Secondary Ion Mass Spectrometry (SIMS) [12]. Even though TDS has provided excellent results, it requires a highly sensitive gas measurement system and is limited by the detection of gases released during annealing only, these being subjected to trapping by defects and grain boundaries.

CONTACT Robert J. W. Frost rob.frost@physics.uu.se Department of Physics and Astronomy, Uppsala University, Box 516, Uppsala SE-751 20, Sweden

Although TDS does allow for a detailed evolution of the gas species distribution in a material to be deduced [13], this evolution is inferred rather than directly measured. SIMS has indeed been used to provide direct measurements of Xe depth-profiles in UO_2 [14], but is a strictly destructive method ablating the sample during measurement. SIMS also suffers from a reliance on accurately known sputter-yields to be quantitative, and depth information must be obtained by independent measurement; optical interferometry, for example. An alternative, and until this time untested, method for measuring elemental depth-profiles in nuclear fuels, is Time-of-Flight – Elastic Recoil Detection Analysis (ToF-ERDA) [15]. Unlike SIMS, ToF-ERDA utilises a high-energy primary-ion beam, in the range of 10's of MeV, which makes sputter yields negligible and results in the technique being non-destructive. As the information provided by ToF-ERDA can be interpreted purely from the perspective of non-relativistic ion scattering, quantitative depth-profiles of all sample constituents can be obtained in a single measurement.

In this rapid communication, the use of ToF-ERDA is presented as an alternative method for tracking the gas mobility in the fuel matrix. For the first time, UO_2 and ADOPT^{TM} samples were tested, and measurements of the ^{84}Kr depth-profiles were performed on samples, both as-implanted and after annealing at 800°C for 1 h. Ultimately the induced changes in the measured depth profiles of ^{84}Kr, in different fuel types, can provide a more fundamental understanding of the diffusion mechanisms. It is worth noting that UO_2 and ADOPT^{TM} were selected as part of a comparative study, due to interest from the nuclear community to understand the gas release properties of ADOPT^{TM}. The addition of Cr_2O_3 and Al_2O_3 at ppm levels [16] in ADOPT^{TM}, results in a significant increase in self-diffusion and there is an ongoing discussion over the full consequences of this for the diffusion of gaseous species [17,18]. Notable differences in fission gas release have been observed for ADOPT^{TM} in comparison with UO_2 specifically in Reactivity-Initiated Accidents (RIAs) scenario [19].

All samples used were discs, 8.6 mm in diameter, cut from fuel pellets provided by Westinghouse Electric Sweden AB. A simplified representation of the sample preparation and experimental set-up used in this work is illustrated in Figure 1. The surface of each disc was ground and polished following 280, 360, 600, 1200 mesh in SiC abrasive paper followed by 9, 6, 3, 1 and 0.25 µm diamond solution with TexMet® (up to 3 µm) and MicroCloth® (Buehler) polishing cloths. The microstructure of UO_2 and ADOPT^{TM} can be seen in the upper section of Figure 2, in which Electron Backscatter Diffraction (EBSD) results are presented. These EBSD data give an average grain size of 8 µm and 30 µm for UO_2 and ADOPT^{TM}

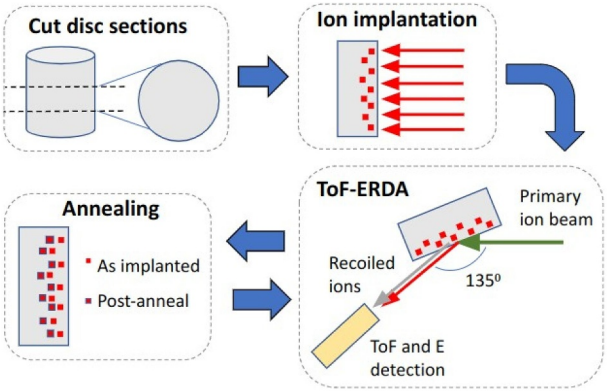

Figure 1. Simplified representation of the sample preparation and experimental sequence.

respectively, with the latter containing enlarged grain size due to the dopants added in fabrication. To predict the depth profile of the implanted ^{84}Kr, the damage to the sample matrix induced by the implantation and the proportion of backscattered ^{84}Kr, simulation was performed using SRIM [20]. This simulation used the *detailed calculation with full damage cascades* performed on 99,999 ions with normal incidence; the results being presented in the lower section of Figure 2. The simulation predicted the proportion of ^{84}Kr backscattered during implantation to be 3.7%. It should be noted that the predicted radiation damage is mainly concentrated within 50 nm of the surface of the samples, which is deeper than the predicted peak in the implanted ^{84}Kr. Diffusion of Kr inward may therefore be less influenced by point defects [21], while Kr diffusing toward the surface may interact with such features.

Ion implantation and ToF-ERDA were performed at the Tandem Laboratory, Uppsala University [22]. All samples were loaded together in the implantation chamber, with the polished surface of each exposed to a beam of $^{84}Kr^{+1}$ ions at 300 keV. The beam configuration was set such that the full surface of each was implanted. Implantation was performed for a period of 5 hours, with the total dose estimated to be 8.5×10^{16} ions/cm^2. The sample holder was water cooled during implantation and did not exceed a temperature of 129°C. First-order calculation shows that, with the implanted fluence used here, Kr atoms will represent more than 10% of the atoms in the sample at the peak of the distribution. In practice, this concentration is never reached due to saturation effects, but as these effects were difficult to predict prior to the experiment, the high fluence was chosen to ensure a significant amount of Kr was retained in the sample. It is important to stress that the peak concentrations of implanted Kr are not representative of typical fission gas concentrations, and should not be regarded as such. The primary goal of the implantation was to create a Kr distribution, over a sufficient

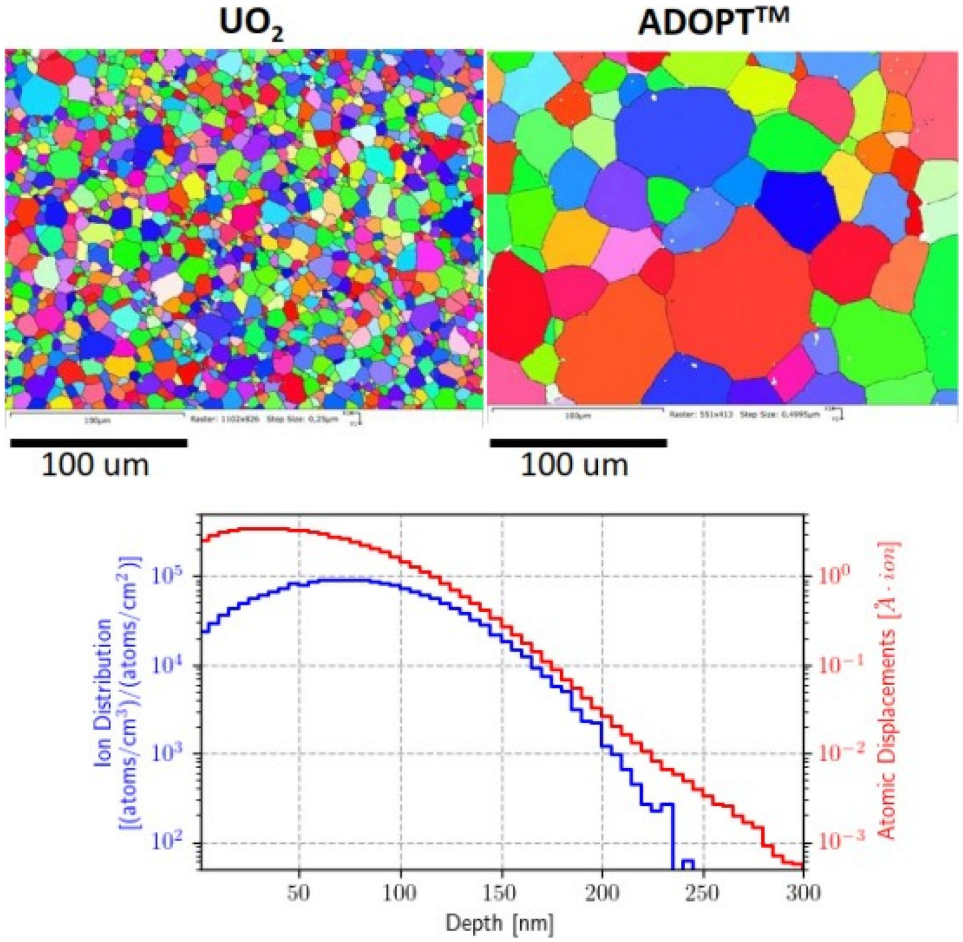

Figure 2. Pre-characterisation and simulation results. Top: EBSD maps of the sample surfaces before ion implantation, from which average grain sizes of 8 µm and 30 µm was obtained for UO_2 and ADOPT™ respectively; bottom: simulation results obtained using SRIM2013 [16], showing the predicted depth profile of ^{84}Kr in UO_2, implanted at 300 keV (blue), and the predicted depth profile of the atomic displacements, induced by the implantation (red).

depth range, that could be easily measured with ToF-ERDA and thus verify the depth-profiling methodology. After implantation, samples of both specimens were subjected to annealing at 800°C for 1 hour. A gas atmosphere of 90%Ar + 10%H_2 was used during the full annealing process, to inhibit UO_2 surface oxidation and deviation from initial stoichiometry. A heating profile of 20°C/min was used for both heating and cooling stages, meaning that the samples spent an additional 80 minutes experiencing a steadily elevated temperature outside of the one-hour annealing time. An approximation for the overall time associated with the diffusion process is therefore inherent to the method used. ToF-ERDA measurements were performed using a beam of 44 MeV $^{127}I^{+8}$ primary ions, incident at 67.5° with respect to the sample surface-normal and recoils were detected at an angle of 45°. The measured surface area of each sample was approximately 1 × 3 mm, the elongation being due to the angle of incidence of the primary-ion beam. The beam current used for the measurements was on the order of 1 nA, and each measurement took ~20- minutes to complete. The ToF-ERDA detector consisted of a time-of-flight telescope followed by a gas ionisation chamber, so that both the energy and time-of-flight of the recoiled particles were recorded [23]. Composition depth profiles from ToF-ERDA measurements were calculated using the CONTES software package [24].

An example ToF-ERDA coincidence spectrum is presented in the top section of Figure 3, with each track in this time-energy plot representing a recoiled or scattered particle mass. It should be noted that the scale of the ToF axis in Figure 3 is inverted, effectively expressing particle velocity. The cut-off of each track at high energy and flight time represents the sample surface, while low energies and flight times for a given track represent recoil events originating from deeper in the sample. For low-mass recoils, close to the surface of the sample, mass separation is at its best and here even isotopic separation is possible. As the mass of the recoils increases, the difference in flight time of similar masses with the same energy reduces and, as such, so does the ability to separate the masses. For recoils originating deep in the sample, significant energy loss occurs and the resulting tracks from nearby masses begin to overlap in the coincidence spectrum, again hindering mass separation. In

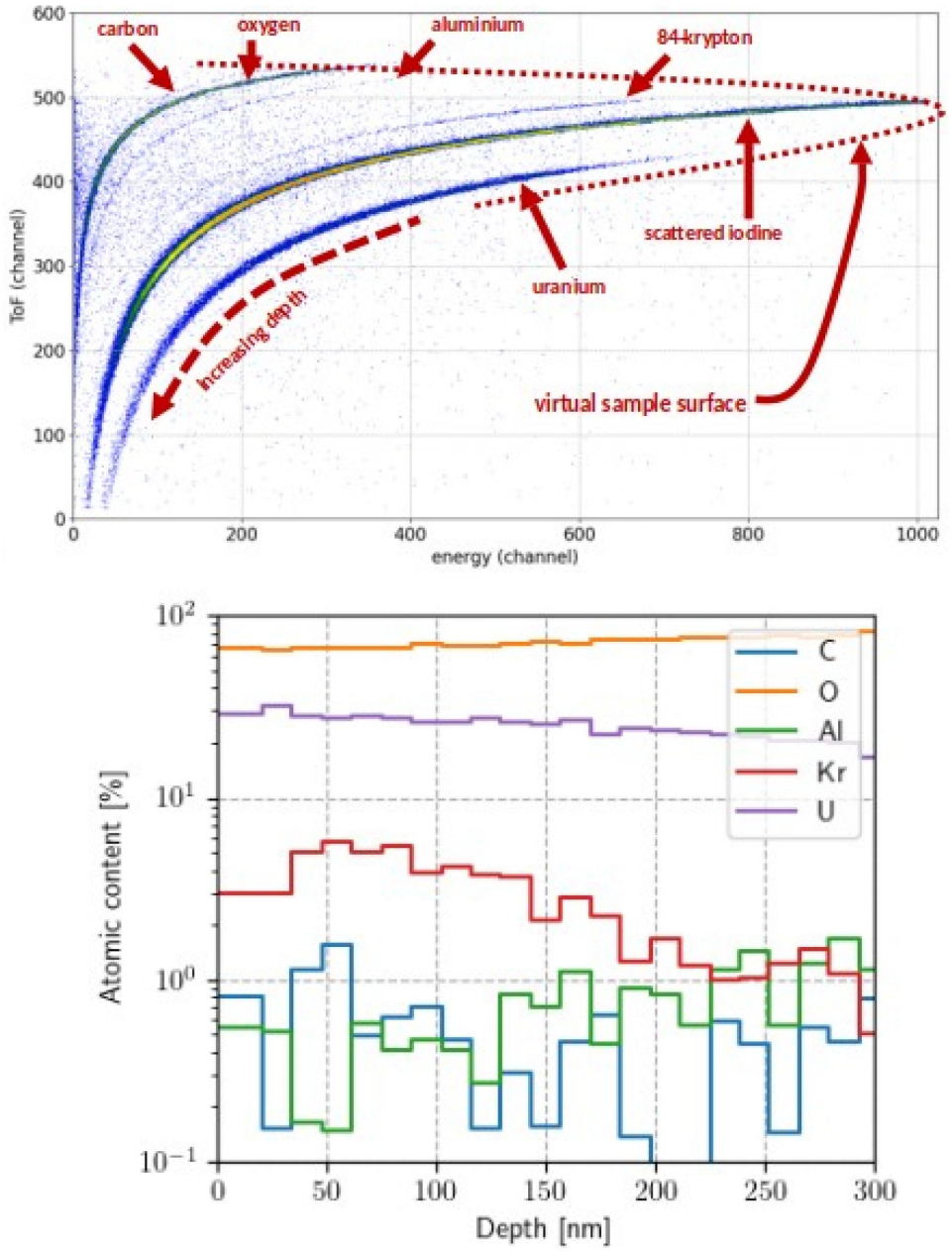

Figure 3. ToF-erda results. Top: ToF-E coincidence plot obtained with ToF-erda, using 44 MeV primary iodine ions for ADOPT^{TM} implanted with ^{84}Kr at 300 KeV. One track is observed for each element detected and one additional track from the scattered primary ions. The "virtual surface" of the sample is marked, events further from this originate from deeper in the sample. Bottom: depth profiles obtained from the ToF-E data, in which the apparent reduction in U concentration with depth is an artefact, caused by multiple scattering in the sample matrix.

Figure 3, the tracks for uranium and oxygen can be clearly distinguished. A track for Al can also be seen, but due to the very low concentrations of Al in ADOPT^{TM} (i.e. tens of ppm), it is likely that this track originates from the primary beam halo impinging on the Al sample holder, the detection limits of the system used being on the order of 0.1 atomic%. Significantly, an isolated band can be seen for ^{84}Kr. The localised concentration of ^{84}Kr, closer to the surface of the sample, can be read from the decreasing intensity of the track at lower energies, relative to the intensity of the track from oxygen, demonstrating the capability of ToF-ERDA to directly measure the elemental depth-profiles of the implanted ions. The elemental depth-profiles, resulting from the analysis of the data in the upper part of Figure 3 are presented in the lower part of Figure 3, in which the depth axis has been scaled to units of nm assuming a constant density of 10.97 g/cm^2. It can be seen from Figure 3, that the majority of as-implanted ^{84}Kr is in the range of approximately 150 nm from the sample surface, this being in agreement with the SRIM simulation results presented in Figure 2 despite the approximation in the conversion of the depth scale. For matrices containing species of high-mass relative to the primary ions, such as U in this case, the primary ions are also scattered into the detection system. This results in the strong track of ^{127}I seen in Figure 3. The scattering of primary

ions into the detector limits the analysis to elements with masses well separated from that of the ion used to probe the sample. If Xe was to be measured for example, this element also being of interest for nuclear fuel performance, an ion beam of Ag or Au would be required to avoid a signal overlap. The apparent reduction in the concentration of U with depth, that can be observed in the lower part of Figure 3 is an artefact, introduced by multiple and plural scattering, of the ion beam and in particular heavy recoiling particles, in the high-mass sample matrix [25,26]. Due to the resulting path length enhancement and additional energy losses, the signals from high-mass recoils are more extensively stretched over a large depth range in the employed evaluation algorithm. This stretching leaves the near-surface signal (~30%) most accurate for the present case. When interpreting the results presented in Figure 3, it should be noted that the artificial reduction in U concentration with depth also artificially inflates the concentrations of all other elements. As this phenomenon is of very similar effect for samples with similar composition however, even subtle changes can be detected when comparing the two different samples. ToF-ERDA is considered to be a non-destructive technique, in that samples do not undergo significant compositional changes and can thus be remeasured and the same results obtained. An exception to this non-destructiveness is when samples containing a significant fraction of light elements (masses less than C) are analysed [27]. Although Kr is far from the mass range that would usually be considered problematic in terms of mass loss during measurement, the list-mode data obtained in this study was analysed to look for systematic changes in the rate Kr ions were registered by the detection system: No such changes were observed.

Figure 4 shows the ^{84}Kr depth-profiles for all samples implanted, both before and after annealing. The differences between the pre- and post-annealed data sets, presented in Figure 4, can be seen to be on a similar order to the statistical uncertainties for each data bin, and as such the present dataset is not sufficient to elucidate a detailed mechanistic understanding of Kr diffusion in each material. Such efforts will be reserved for more extensive future studies. Nevertheless, the variations between and within these data sets are sufficient to be indicative of the possible mechanisms at play. The near-surface portion of the^{84}Kr profiles, in front of the peak in the distributions, is reasonably constant for all three samples before and after annealing. For UO_2, the major shift in the distribution is seen to result from the movement of Kr from deeper within the sample, at greater than 150 nm. Given the smaller grain size and consequently shorter diffusion lengths of UO_2 relative to ADOPT^{TM}, it is probable that a tendency of UO_2 to vent is being observed. For the ADOPT^{TM} samples, there is no significant movement of the ^{84}Kr observed deeper than 200 nm, the only notable change in distributions being a flattening from the peak down to around 200 nm. This flattening points to limited venting of the implanted Kr. When integrating across the

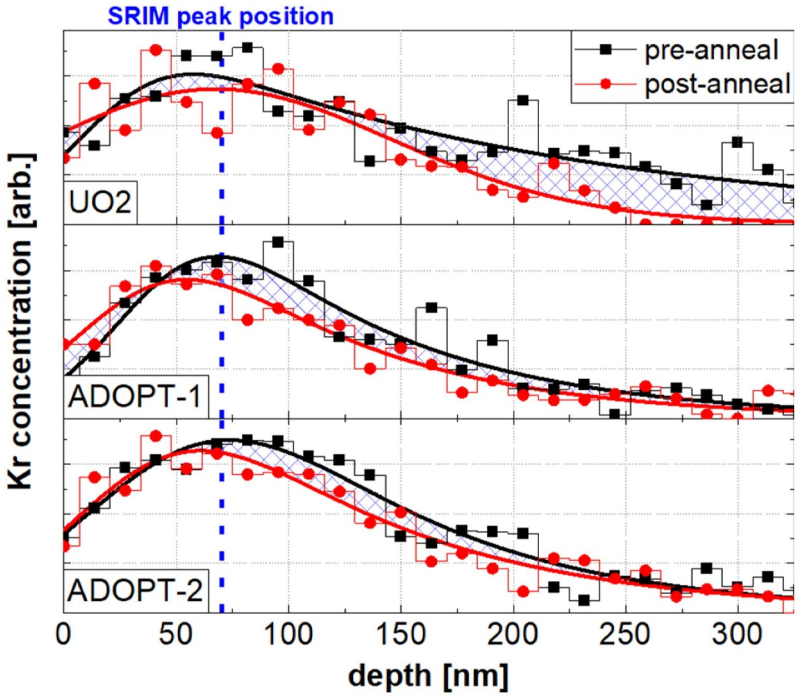

Figure 4. A comparison of the ^{84}Kr depth-profiles in each sample, both before and after annealing. Fits to the data were made with a modified Gaussian function. The maxima of the as-implanted ^{84}Kr concentration predicted by SRIM is indicated. Although arbitrary Kr concentrations are indicated on the main-figure axis, no normalisation has been applied between the data within each subplot, and the differences shown between the pre- and post-anneal Kr profiles for each sample are absolute.

distributions for each sample, the total reduction in areal density of ^{84}Kr following annealing, is found to 25% for UO_2, while just 13% and 10% for ADOPT-1 and ADOPT-2 respectively. It is notable that great consistency is observed in the Kr distributions in the two ADOPT^{TM} samples, which then show a marked difference to the distributions seen in UO_2. It is therefore likely that two distinct behaviours are observable in these data: enhanced venting in UO_2, stemming from smaller grain size, and enhanced diffusion in ADOPT^{TM} offset by larger grain size and longer path lengths. These observations therefore correlate with the consensus on the diffusion of Kr in standard UO_2 vs doped UO_2 fuels such as ADOPT^{TM} [16,18,28,29]. When considering the possible diffusion mechanisms at play in this study, it is important to note the high microstructural damage induced by the implantation procedure. This damage is predicted, as shown in Figure 2, to be around 5 dpa/Å·ion at peak or, considering the implanted fluence of 8.5×10^{16} ions, around 500 dpa. Such damage could potentially lead to enhanced diffusion caused by microstructural and crystalline defect repair during annealing. However, given the identical implantation and annealing conditions for all samples, and in particular the relatively low temperatures used in the latter, it is considered that these experimental artefacts have not affected one sample over the others.

Using a combination of noble-gas ion implantation and ToF-ERDA, it was possible to resolve differences in the outgassing behaviours between UO_2 and ADOPT^{TM} fuels when subjected to implantation and annealing. While the present study lacks a sufficient breadth and scale to provide a clear mechanistic understanding of the observed differences, the results obtained stand in agreement with the current consensus on the behaviour of the fuels studied. Furthermore, the approach taken in this work represents a novel technique for the direct measurement of noble-gas diffusion in unirradiated nuclear fuel. The use and continued development of such a technique promises the ability to dramatically increase the throughput of measurements at a significantly reduced costs and timescale compared to traditional methods, such as base irradiation, test irradiation, MTR, and Hot-cell-based methods. To enable this, work is already underway [30] to optimise ToF-ERDA measurement parameters, such as type and energy of the primary ion used, for these very heavy sample matrices. Future measurement campaigns on reactor fuels will focus on the collection of greater statistics, both in terms of individual measurements and the number of samples analysed. These future campaigns will also include: varying concentration of the implanted ions; varying the depth of the implanted ions; implantation at different temperatures; annealing samples under various temperatures, up to 1600°C; and ultimately *in situ* studies, in which elemental depth-profiles will be measured during annealing. These broadened methodologies will be further employed for the collection of similar data on other elemental species of interest, such as semi-volatile fission products like Cs, I, as well as solid fission products like Mo, Ru, Pd. These methodologies will then be readily applicable to studies of novel fuel matrices such as UC, UN, and other ATF and Generation IV materials, and can therefore significantly aid in improving the mechanistic understanding of fuel performance, material development and qualification.

Acknowledgments

Financial support from Studsvik Nuclear AB within the framework of the ANItA Centre is gratefully acknowledged, as is the financial support from The Swedish Strategic Research Foundation (SSF) within the SUNRISE-project and the financial support from the Swedish Research Council (VR-RFI) under contract number 2019-00191.

Disclosure statement

No potential conflict of interest was reported by the author(s).

Funding

This work was supported by the Vetenskapsrådet [VR-RFI -2019-00191].

References

[1] Bailly H, Menissier D, Prunier C. The nuclear fuel of pressurized water reactors and fast reactors: design and behavior. Intercept; 1999.
[2] Ferry C, Poinssot C, Broudic V, et al. Synthesis on the spent fuel long term evolution. CEA; 2005. CEA-R-6084.
[3] Jernkvist LO. A review of analytical criteria for fission gas induced fragmentation of oxide fuel in accident conditions. Prog Nucl Energy. 2020;119:103188. doi: 10.1016/j.pnucene.2019.103188
[4] Turnbull J, Friskney C, Findlay J, et al. The diffusion coefficients of gaseous and volatile species during the irradiation of uranium dioxide. J Nucl Mater. 1982;107(2):168–184. doi: 10.1016/0022-3115(82)90419-6
[5] Lawrence G. A review of the diffusion coefficient of fission-product rare gases in uranium dioxide. J Nucl Mater. 1978;71(2):195–218. doi: 10.1016/0022-3115(78)90418-X
[6] Terrani KA, Capps NA, Kerr MJ, et al. Accelerating nuclear fuel development and qualification: modeling and simulation integrated with separate-effects testing. J Nucl Mater. 2020;539:152267. doi: 10.1016/j.jnucmat.2020.152267
[7] Hales J, Novascona S, Pastore G, et al. BISON theory manual: the equations behind nuclear fuel analysis. Idaho National Laboratory; 2013. INL/EXT-13–29930.

[8] Pastore G, Luzzi L, Di Marcello V, et al. Physics-based modelling of fission gas swelling and release in UO2 applied to integral fuel rod analysis. Nucl Eng Des. 2013;256:75–86. doi: 10.1016/j.nucengdes.2012.12.002
[9] Tonks M, Andersson D, Philipot S, et al. Mechanistic modelling for nuclear fuel performance. Ann Nucl Energy. 2017;105:11–24. doi: 10.1016/j.anucene.2017.03.005
[10] Gerardin M, Gilabert E, Horlait D, et al. Experimental study of the diffusion of xe and kr implanted at low concentrations in UO2 and determination of their trapping mechanisms. J Nucl Mater. 2021;556:153174. doi: 10.1016/j.jnucmat.2021.153174
[11] Gerardin M, Gilabert E, Horlait D, et al. Diffusion of Xe and Kr implanted at low concentrations in UO2 as a function of temperature – an experimental study. J Nucl Mater. 2023;582:154476. doi: 10.1016/j.jnucmat.2023.154476
[12] Peres P, Choi SY, Desse F, et al. Dynamic SIMS for materials analysis in nuclear science. J Vac Sci Technol B. 2018 02;36(3):03F117. doi: 10.1116/1.5017027
[13] Horlait D, Domange J, Amany ML, et al. Experimental investigation of Kr diffusion in UO2 +x: slight deviations from stoichiometry, significant effects on diffusion kinetics and mechanisms. J Nucl Mater. 2023;574:154191. doi: 10.1016/j.jnucmat.2022.154191
[14] Marchand B, Moncoffre N, Pipon Y, et al. Xenon migration in UO2 under irradiation studied by SIMS profilometry. J Nucl Mater. 2013;440(1):562–567. doi: 10.1016/j.jnucmat.2013.04.005
[15] Avasthi DK, Assmann W. ERDA with swift heavy ions for materials characterization. Curr Sci. 2001;80(12):1532–1541.
[16] Arborelius J, Backman K, Hallstadius L, et al. Advanced doped UO2 pellets in LWR applications. J Nucl Sci Technol. 2006;43(9):967–976. doi: 10.1080/18811248.2006.9711184
[17] Killeen J. Fission gas release and swelling in UO2 doped with Cr2O3. J Nucl Mater. 1980;88(2):177–184. doi: 10.1016/0022-3115(80)90272-X
[18] Cooper M, Pastore G, Che Y, et al. Fission gas diffusion and release for Cr2O3-doped UO2: from the atomic to the engineering scale. J Nucl Mater. 2021;545:152590. doi: 10.1016/j.jnucmat.2020.152590
[19] Brown N, Wysocki A, Terrani K, et al. The potential impact of enhanced accident tolerant cladding materials on reactivity initiated accidents in light water reactors. Ann Nucl Energy. 2017;99:353–365. doi: 10.1016/j.anucene.2016.09.033
[20] Ziegler J, Biersack J, Littmark U. SRIM – the stopping and range of ions in matter (2008). Nucl Instrum Methods Phys Res Sect B Beam Interact Mater Atoms. 2010;268(11–12):1818–1823. doi: 10.1016/j.nimb.2010.02.091
[21] Wang L, Zhen W, Yaping X, et al. Effects of point defects on the stable occupation, diffusion and nucleation of Xe and Kr in UO2. Metals. 2022;12(5):789. doi: 10.3390/met12050789
[22] Ström P, Primetzhofer D. Ion beam tools for nondestructive in-situ and in-operando composition analysis and modification of materials at the tandem laboratory in Uppsala. J Inst. 2022;17(4):04011. doi: 10.1088/1748-0221/17/04/P04011
[23] Ström P, Petersson PRMPD, Brezinsek S, et al. Ion beam analysis of tungsten layers in EUROFER model systems and carbon plasma-facing components. Nucl Instrum Methods Phys Res Sect B Beam Interact Mater Atoms. 2016;371:355–359. doi: 10.1016/j.nimb.2015.09.024
[24] Janson MS. CONTES instruction manual. Internal report. Uppsala University; 2004.
[25] Pitthan E, Moro M, Correa S, et al. Assessing boron quantification and depth profiling of different boride materials using ion beams. Surf Coat Technol. 2021;417:127188. doi: 10.1016/j.surfcoat.2021.127188
[26] Kantre K, Moro MV, Petersson VP, et al. Assessing electronic energy loss of heavy ions detected in reflection geometry. Surf Interface Anal. 2021;53(7):650. doi: 10.1002/sia.6951
[27] Adel M, Amir O, Kalish R, et al. Ion-beam-induced hydrogen release from a-c: h: a bulk molecular recombination model. J Appl Phys. 1989;66(7):3248–3251. doi: 10.1063/1.344116
[28] Rest J, Cooper MWD, Spino J, et al. Fission gas release from UO2 nuclear fuel: a review. J Nucl Mater. 2019;513:310–345. doi: 10.1016/j.jnucmat.2018.08.019
[29] Tonks M, Andersson D, Devanathan R, et al. Unit mechanisms of fission gas release: current understanding and future needs. J Nucl Mater. 2018;504:300–317. doi: 10.1016/j.jnucmat.2018.03.016
[30] Frost RJW, Lopes DA, Johnson KD, et al. The optimisation of ToF-ERDA for elemental depth-profiling in very-heavy sample matrices. Manuscript in preparation. 2023.